Centre of Excellence for Pharmaceutical Sciences (Pharmacen), North-West University, Potchefstroom, South Africa

Exploratory data analysis of the dependencies between skin permeability, molecular weight and log P

D. Kilian, H.J.R. Lemmer, M. Gerber, J.L. du Preez, J. du Plessis

Received October 10, 2015, accepted January 12, 2016

Jeanetta du Plessis, Centre of Excellence for Pharmaceutical Sciences (Pharmacen), North-West University, Private Bag X6001, Potchefstroom 2520, South Africa
Jeanetta.duPlessis@nwu.ac.za

Pharmazie 71: 311–319 (2016) *doi: 10.1691/ph.2016.5170*

Molecular weight and log P remain the most frequently used physicochemical properties in models that predict skin permeability. However, several reports over the past two decades have suggested that predictions made by these models may not be sufficiently accurate. In this study, exploratory data analysis of the probabilistic dependencies between molecular weight, log P and log *Kp* was performed on a dataset constructed from the combination of several popular datasets. The results suggest that, in general, molecular weight and log P are poorly correlated to log *Kp*. However, after employing several exploratory data analysis techniques, regions within the dataset of statistically significant dependence were identified. As an example of the applicability of the information extracted from the exploratory data analyses, a multiple linear regression model was constructed, bounded by the ranges of dependence. This model gave reasonable approximations to log *Kp* values obtained from skin permeability studies of selected non-steroidal ant-inflammatory drugs (NSAIDs) administered from a buffer solution and a lipid-based drug delivery system. A method of testing whether a given drug falls within the regions of statistical dependence was also presented. Knowing the ranges within which molecular weight and log P are statistically related to log *Kp* can supplement existing methods of screening, risk analysis or early drug development decision making to add confidence to predictions made regarding skin permeability.

1. Introduction

Over the past 50 years, *in vitro* skin permeability studies had become a major research topic in various fields, ranging from pharmaceutical sciences to cosmetics and risk assessment (Fitzpatrick et al. 2004; Hadgraft and Lane 2005; Shen et al. 2014). From a pharmaceutical perspective, transdermal delivery offers an attractive alternative to other routes of administration. Advantages include the ease of application and elimination of gastric side-effects, both of which can improve patient compliance, as well as bypassing of the first-pass metabolic effect (Hadgraft and Lane 2005). The latter can potentially lower the amount of drug needed to elicit the same therapeutic response obtained from other routes of administration, which may in turn decrease the cost of the formulation and potentially increase the availability of drugs to aid organizations and poorer countries.

Among the most important factors that determine a drug's ability to permeate the skin are its physiochemical properties. These, along with the drug's biopharmaceutical characteristics, are used extensively in drug discovery and development decision making (Bharate and Vishwakarma 2013). Popular classification systems for selecting favorable drug candidates for oral delivery include the biopharmaceutical classification system (BCS) and Lipinski's rule of five (Amidon et al. 1995; Lipinski et al. 2001). However, when it comes to transdermal delivery, reaching an agreement on which physicochemical properties, and in what ranges, to use for classification becomes more complicated. Molecular weight (MW), aqueous solubility, melting point and oil/water partition coefficient (log P) have been suggested as important indicators of skin permeability (Roy 1997), with nondescriptive "cut-off" points, like a MW of less than 600 Da (Daltons), good solubility both in oil and water, and a low melting point (Barry 2001). Referring back to Lipinski's rule of five, we find that this classification system selects favorable drug candidates based on the following criteria: (1) no more than 5 H-bond donors, (2) at most 10 H-bond acceptors, (3) a maximum MW of 500 Da and (4) a log P value not higher than 5. Because the stratum corneum forms a more formidable barrier than the intestinal epithelium, some studies caution against the direct use of the rule of five to identify potential drug candidates for transdermal delivery (Choy 2011). Most authors, however, agree that the rule of five is still applicable to transdermal delivery, as long as some restrictions are placed on the physicochemical properties' selection criteria. These restrictions include the addition of a lower boundary for the log P values, i.e. log P ≥ 0, with optimal values at around 2 to 3, as well as a lowering of the upper boundary of MW to between 400 and 500 Da, with ideal values below 400 Da and optimal values at around 150 Da (Choy 2011; Bos and Meinhardi 2000; Magnusson et al. 2004; Wiedersberg and Guy 2014).

In the absence of definitive physicochemical property ranges for classifying potential transdermal drug candidates, many researchers turn to the skin permeability constant, *Kp*, as an indicator of expected skin permeability. Under steady state conditions (within the stratum corneum), *Kp* can be expressed as the proportionality constant between the steady state flux and concentration gradient of a solute across the stratum corneum (Scheuplein 1965). While *Kp* has value in its own right, it may also be used to calculate the maximum flux, *Jmax*, of a solute, which many researchers deem to be of the most practical interest when investigating maximal transdermal uptake (Cooper 1986; Lippold 1991; Le and Lippold 1995; Magnusson et al. 2004). Mathematical methods that predict *Kp* include quantitative structure-permeability relationship (QSPR) models (Moss et al. 2002), artificial neural networks (Chen et al. 1993), random walks (Frasch 2002) and mechanistic models combining different transdermal routes and free-volume theory (Mitragotri 2002). QSPR models specifically have seen extensive use in transdermal permeability studies. From the early to mid-1990's, several of these multiple linear regression models were developed in an attempt to estimate the *Kp* value of a chemical entity directly from certain physicochemical properties, most commonly molecular size and log P (Abraham et al. 1995; Barrat

1995; Lien and Gao 1995; Potts and Guy 1992, 1995; Wilscut et al. 1995). Numerous QSPR models have been developed since then (Bouwman et al. 2008), and are still being developed, mainly because of the poor predictions associated with applying these models to datasets other than the ones used to derive them. In a study by Lian et al. (2008) the predictive accuracy of several popular QSPR models, and Mitragotri's model, was investigated using a dataset containing experimental log *Kp* values of 124 compounds. Some of the models returned R^2 values as low as 0.364 and 0.463, while R^2 values as low as 0.159 were reported when restricting the dataset to hydrophobic solutes. It should also be noted that even in the original QSPR model by Potts and Guy (1992) only about two thirds of the variance in skin permeability data could be explained by the model ($R^2 = 0.67$). However, a detailed discussion on the mathematical and statistical methods used to derive and validate these models is not the purpose of this study. Rather, we will take the two structural descriptors most frequently used in transdermal permeability studies, i.e. molecular size and log P, and investigate the probabilistic dependencies between these variables and the skin permeability constant.

In this study, MW was used as the molecular size descriptor. However, a comparison between the MW and molecular volumes (MV) of the drugs in the dataset showed that these two properties are strongly correlated, with R^2 and adjusted R^2 values of 0.92 (see supplementary information). They might therefore be reasonably interchangeable, following the appropriate multiplications. Because of the ease of calculating MW, and its frequent use in QSPR models, it was chosen for this study. By combining datasets from several previous studies, a dataset larger than any previously reported was constructed. Several exploratory data analysis techniques were used to extract information from this dataset. Finally, a skin permeability study of selected non-steroidal anti-inflammatory drugs (NSAIDs), dissolved in phosphate buffer solution (PBS), and dispersed in a lipid-based drug delivery system, was conducted. The Pheroid™ was chosen as the lipid-based drug delivery system for this study. It is a colloidal delivery system, consisting of essential and plant fatty acids that, for the current study, had been emulsified in PBS saturated with nitrous oxide, to produce liposome-like bilayer vesicles with mean diameters of ~1 µm (Du Plessis et al. 2010). The ability of the Pheroid™ to entrap and delivery drugs over different biological membranes has been reported (Du Plessis et al. 2010), and one of its earliest uses was as a skin penetration enhancer (Saunders et al. 1999).

2. Investigations and results

The correlation matrices of the individual and combined datasets are presented in Table 1. The results suggest that MW and log P are not strongly correlated to log *Kp*, and may not be the best choice of independent variables in quantitative models. To assist

Table 1: Correlation matrices of the datasets used in this study, Lian *et al*. (A), Moss and Cronin (B), Wilscut et al. (C) and the combined set (D)

A				**B**			
	MW	log P	log *Kp*		MW	log P	log *Kp*
MW	1.0000	0.4085	-0.2852	MW	1.0000	0.4548	-0.2515
log P	0.4085	1.0000	0.5983	log P	0.4548	1.0000	0.6214
log K_p	-0.2852	0.5983	1.0000	log K_p	-0.2515	0.6214	1.0000
C				**D**			
MW	1.0000	0.2617	-0.4248	MW	1.0000	0.3716	-0.2105
log P	0.2617	1.0000	0.4913	log P	0.3716	1.0000	0.2783
log K_p	-0.4248	0.4913	1.0000	log K_p	-0.2105	0.2783	1.0000

in visualizing the data contained in the correlation matrices, scatterplot matrices of the datasets are presented in Figure 1. The cells on the main diagonals contain the smoothed histograms of the corresponding random variables. From this visual representation of the datasets, several interesting observations emerged. First, the distributions of the molecular weights of substances tested for transdermal delivery were consistently positively skewed. Also, despite several previous papers claiming an upper cut-off boundary for MW to be 500 Da (see introduction), we see that very little data is actually available above this region. Probably the most interesting, and troubling observation is that the increase in dataset size elucidated a bimodal distribution in log *Kp*, suggesting that the same ranges of MW and log P that correspond to "good" log *Kp* values also correspond to "poor" ones.

Before continuing, let's first revisit the rationale behind the use of molecular weight and log P as estimators for transdermal permeability. Under steady state conditions, i.e. when the stratum corneum is saturated with solute, Fick's first law of diffusion can be expressed as (Scheuplein 1965):

$$J_{ss} = K_p \Delta C_s = \frac{K_{mv} D}{h} \Delta C_s \quad (1)$$

where *Jss* is the steady state flux, *D* the diffusion coefficient, Δ*Cs* is the molar concentration gradient across the skin membrane, *Kmv* is the membrane/vehicle partition coefficient and h is the thickness of the skin membrane. Therefore, *Kp*, can then be expressed as:

$$K_p = \frac{K_{mv} D}{h} \quad (2)$$

If we make the assumption that the solute concentration is essentially zero on one side of the skin, *Kmv* can simply be expressed as the ratio of solute concentration in the skin to the solute concentration in the vehicle, *Kmv* = *Cs*/*Cv*, and can be substituted with *Kow*, the octanol/water partition coefficient (Potts and Guy 1992). Since *D* can also be difficult to calculate, a further assumption is made that *D* can be expressed as a negative exponential function of molecular size, based on an adaptation to the free volume theory of solute diffusion through polymers (Potts and Guy 1992):

$$D = D_0 e^{-\beta MV} \quad (3)$$

where D_0 is the diffusivity of an infinitesimally small (zero volume) molecule and β is a constant. This expression is dissimilar to the Stokes-Einstein equation, where D is inversely proportional to molecular size, expressed as molecular radius:

$$D = \frac{RT}{6\pi N_A \eta r} \quad (4)$$

where *R* is the gas constant, *T* is the temperature in Kelvin, *NA* is Avogadro's number, η is the viscosity of the medium through which the compound diffuses and *r* is the molecular radius, which can be calculated directly from MW and the compound's density, ρ, using:

$$r = \left(\frac{3MW}{4\pi\rho N_A} \right)^{1/3} \quad (5)$$

It has been postulated that Eq. (3) can be used to express diffusivity through the stratum corneum (Potts and Guy 1992; Mitragotri et al. 2011), while Eq. (4) can be used to express diffusivity through porous and shunt pathways, the latter consisting of hair follicles and sweat ducts (Mitragotri 2003). It is therefore conceivable that the actual diffusivity could consist of different ratios of the Eq. (3) and (4), and possibly other diffusion coefficients. Incorporating the above mentioned assumptions into Eq. (2), and performing a logarithmic transformation, gives the general form of the QSPR models as:

$$\log K_p = \alpha \log K_{ow} - \frac{\beta MW}{2.303} + \log \frac{D_0}{h} \quad (6)$$

where α is a constant and log *Kow* is the same as log P. Similarly, the general form of Mitragotri's scaled particle theory model (2002) can be expressed as:

$$K_p = \frac{D_{lip} K_{mv}}{\delta h} = K_{ow}^n \cdot \exp\left(-\beta r^2\right) \cdot \frac{D_0}{\delta h} \quad (7)$$

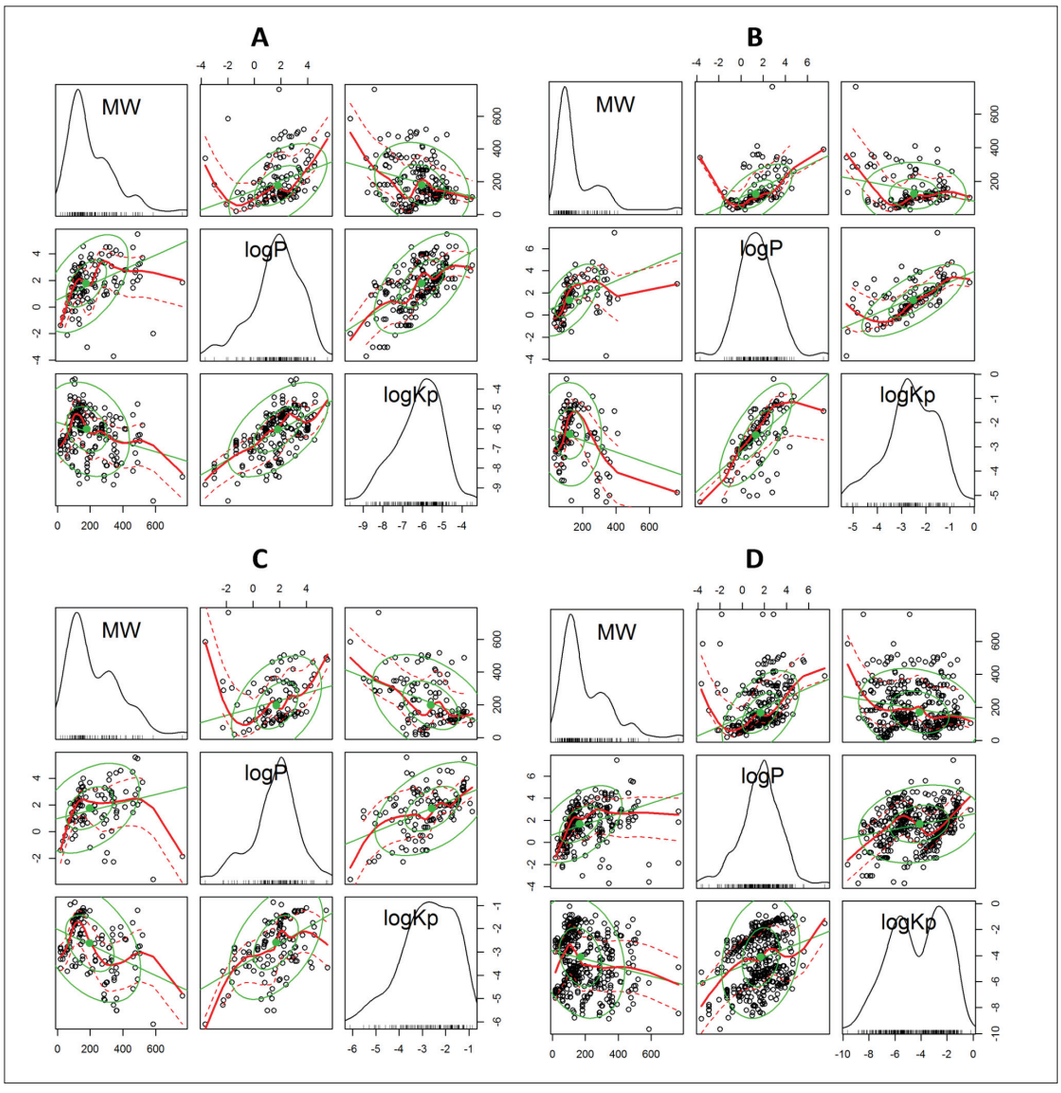

Fig. 1: Scatterplot matrices of the datasets of Lian et al. (**A**), Moss and Cronin (**B**), Wilscut et al. (**C**) and the combined set (**D**).

where τ is the effective tortuosity, *r* is the molecular radius and *Kow* is related to *Kmv* through *Kmv* = *Kown*, where *n* can vary between 0.70 and 0.86. Despite the simplifying assumptions described above, and the poor correlations seen from the correlation matrices, log P and MW remain the mainstay structural descriptors used by pharmaceutical scientists for steady state transdermal permeability predictions. We will therefore investigate whether we can extract valuable skin permeability information from these two variables by applying the appropriate statistical methods. The first task was to determine whether the poor correlations seen in Table 1 were the result of the entire dataset, or just "pockets" of independence within the dataset. To this end, tests for statistical independence were implemented.

2.1. Statistical independence tests

Because of the severe deviation from normality in the data (Fig. 1), it was decided to change the data from continuous to ordinal categorical variables. Initial attempts to discretize the data using Hartemink's Information-Preserving Discretization (IPD) algorithm were unsuccessful (Hartemink 2001). The spread of the data lead to disproportionately large size allocations to areas where the data was sparse, while allocating small regions to areas where the data was clustered. It was therefore decided to cut the continuous data into intervals, chosen *a priori*, based on literature described in the introduction and prior knowledge of the field. Details on the selection of cut-off values are presented in the experimental section. The regions into which the data was split, along with each region's ordinal value, are presented in Table 2.

Table 2: Cut-off points for the data discretization and ordinal values attributed to each region

MW				
≤ 100	(100, 200]	(200, 300]	(300, 400]	> 400
1	2	3	4	5
log P				
≤ 0	(0, 2]	(2, 4]	> 4	
1	2	3	4	
log *Kp*				
≤ -7	(-7, -5]	(-5, -3]	(-3, -1]	> -1
1	2	3	4	5

A detailed 3-way contingency table of the combined dataset was set up. To assist in visualizing this table, a mosaic plot of the data was constructed and presented in Fig. 2. The mosaic plot was also used to test for independence. For the Pearson residuals, which are ~N(0,1) distributed, α = 0.0500 and α = 0.0001 levels of significance correspond to absolute residual values of 2 and 4, respectively, as seen along the right side of Fig. 2. These residuals were used to

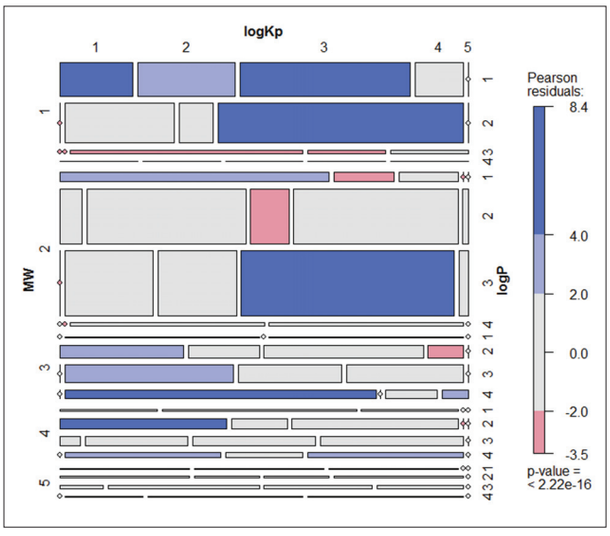

Fig. 2: Mosaic plot of the combined dataset, shaded based on Pearson residual values.

test for significant differences between the cells of the expected values mosaic plot, i.e. independence, and the plot constructed from the 3-way contingency table (Fig. 2). More than half of the cells did not differ from the null model (expected values mosaic plot) by a statistically significant margin, indicating that no statistically significant dependence exists among the variables within these regions. For the dataset as a whole, Pearson's Chi-square test was used to test for independence. The test statistic was significantly larger than the critical value, $\chi^2 > \chi^2\alpha = 248.000 > 97.351$, allowing us to reject the null hypothesis at the 5% level of significance and conclude that the variables in the dataset are not independent. The poor correlations observed from the correlation matrices in Table 1 are therefore rather the result of "pockets" of independence between the variables in the dataset, i.e. the grey cells in Fig. 2.

Because of the low probability of observing log *Kp* values > -1 (from contingency table), a more realistic region to be classified as good transdermal permeability is log *Kp* = (3, 1], or log *Kp* = 4 from Table 2. From the mosaic plot, we see that the frequency of observing log *Kp* values in the ordinal range 4 is significantly higher than expected in the two regions, MW = 2, log P = 3 and MW = 1, log P = 2. The question might now arise: which one of these regions of dependence is the better classifier, or are both equally good? One way to attempt to answer this question is to calculate the individual conditional probabilities of observing a drug with a log *Kp* value within region 4, given that it had MW and log P values within the regions specified above, i.e. 2, 3 and 1, 2, respectively.

2.2. Total probability and Bayes' Rule

If we let B denote the event where a drug displayed a log *Kp* value within one of the regions given in Table 2, such that the sample space Ω can be given by , and let A denote the event where a drug had a MW and log P within the regions specified above, then the law of total probability gives

$$P(A) = \sum_{i=1}^{5} P(A|B_i)P(B_i) \tag{7}$$

The conditional probability of observing a drug within the region log *Kp* = 4, given that it had MW and log P values within the regions, MW = 1, log P = 2, can be calculated using Bayes' Rule:

$$P(B_4|A) = \frac{P(A|B_4)P(B_4)}{\sum_{i=1}^{5} P(A|B_i)P(B_i)} \tag{8}$$

The conditional probability obtained was 0.425. However, the conditional probability of observing a drug within the region log *Kp* = 4, given that it had MW and log P values within the regions, MW = 2, log P = 3, was calculated to be 0.185, which is much lower than expected. The reason for this is that two of the five drugs that displayed log *Kp* values > -1 were within this MW and log P region, giving *P*(*A*|*B5*) = 0.4. If not for this, the MW and log P regions, MW = 2, log P = 3, might be considered equal or better than MW = 1, log P = 2, since P(log *Kp* = 4 | MW = 2, log P = 3) = 0.299, whereas P(log *Kp* = 4 | MW = 1, log P = 2) = 0.233. With the law of total probability and Bayes' Rule failing to give an adequate indication of which joint MW and log P region are associated with the highest probability of observing a log *Kp* value within region 4, we turn to a different multivariate statistical technique, called correspondence analysis, which is conceptually similar to principle component analysis but differs in that it applies to categorical rather that continuous data.

2.3. Correspondence analysis

For brevity, only summarized results and the correspondence map (Figure 3) will be discussed here. Results from the correspondence analysis can be obtained from the authors on request. The total inertia was larger than the χ^2 critical value at the 5% level of significance, allowing us to conclude that the variables are generally not independent. This corroborates the results from the χ^2 test for independence performed on the dataset in section 2.1. From

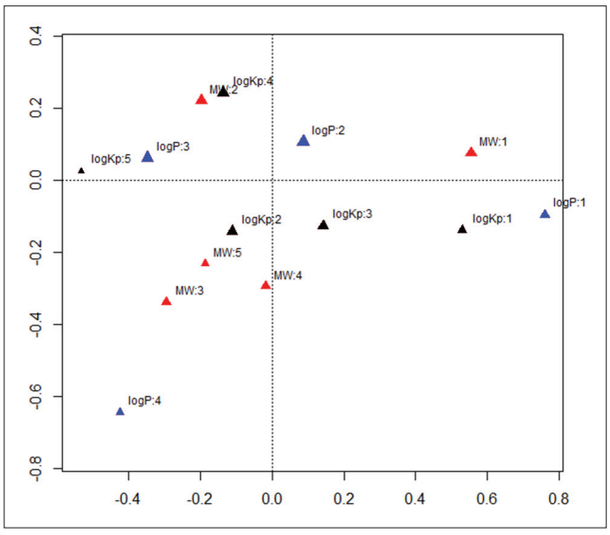

Fig. 3: Correspondence map of the categorical variables. The size of the points indicates the mass of the variable. Dimension 1 is plotted on the horizontal axis and dimension 2 on the vertical axis.

the correspondence map we can see that no single variable differs significantly, as a group, from the other variables. MW made the largest contribution to the total inertia, with the first axis (vertical line) opposing medium and large MWs to MWs smaller than 100 Da. The second axis (horizontal line) opposes medium regions of log P to large and negative regions, and also opposes "good" log *Kp* regions, 4 and 5, from poor regions. The correspondence map suggests that the frequency of observing good skin permeability constants, log *Kp* = 4 and 5, are higher than expected in the regions MW = 2 and log P = 3, respectively. Also, poor skin permeability constant values, log *Kp* = 2, are observed more frequently in high MW regions, MW = 5, while the poorest values, log *Kp* = 1, are observed more frequently than expected with negative log P values. These isolated occurrences of higher than average observation frequency tendencies are consistent with those observed from the mosaic plot. The results from the correspondence analysis seems to answer the question concerning which joint MW, log P range is most likely to correspond to log *Kp* values in the range (3, 1], namely MW = (100, 200] and log P = (2, 4].

The results thus far suggest that, despite the overall poor correlations between the variables in the dataset, regions of statistically significant dependence exist and can be used to determine which observations have a higher than expected frequency of being observed together. It was therefore decided to perform a cluster analysis on the initial, continuous data, to obtain higher resolutions on the bounds of the dependent regions.

2.4. Cluster analysis

Because of the severe departure from normality in the distributions of MW and log *Kp*, it was decided not to use model-based clustering. Instead, we investigated clustering via nonparametric density estimation (Azzalini 2007; Menardi 2014). Details of the cluster analysis procedure are explained in the experimental section. The results of the cluster analysis are presented in Fig. 4, while additional diagnostic plots can be found in the supplementary information.

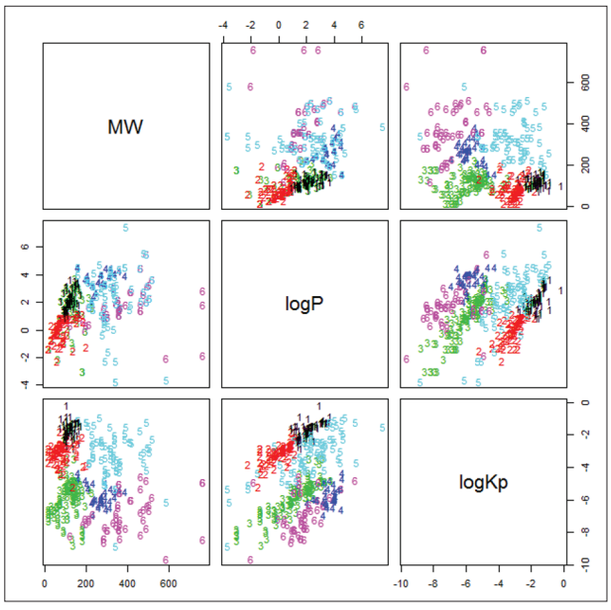

Fig. 4: Results of the estimated density cluster analysis, showing the clustering of the groups into which the dataset were divided, group 1 – black, 2 – red, 3 – green, 4 – blue, 5 – turquoise, 6 – purple, as well as the cluster tree.

The cluster analysis identified six groups, with the smallest dissimilarity between groups 1 and 2. These groups consisted of molecules with MW averages of 128.18±65.693 and 135.06±116.327 Da, log P averages of 1.57±1.486 and 1.01±1.54, and log *Kp* averages of -2.36±1.113 and -2.76±0.942 for groups 1 and 2, respectively. The ranges of the variables in groups 1 and 2 coincide with the two statistically dependent sets of ranges identified with the previous analyses. With the identification of groups 1 and 2, and their location within the regions of statistical dependence, we now investigate the applications of the information extracted from the dataset.

2.5. Multiple linear regression analysis

Quantitative forecasting models remain an attractive predictive technique, due to its usability by a wide range of scientists regardless of their mathematical proficiency. The clade of groups 1 and 2 was used to construct a smaller dataset, consisting only of variable ranges within which the variables are statistically dependent. The ranges of these variables were MW = [18, 336.47], log P = [-2.26, 4.57] and log *Kp* = [-5.22 -0.85]. Employing least squares techniques on this new dataset gave the following multiple linear regression model:

$$\log K_p = 0.739 \log P - 0.0089 \mathrm{MW} - 2.36 \quad (9)$$

The coefficients of determination for the model were $R^2 = 0.856$ and adjusted $R^2 = 0.854$. However, one should not expect R^2 values much higher than these, since the model is constructed from regions of mutual dependence between all the variables, and one must therefore be mindful of the multicollinearity that will be present in the model. Details on the model fitting diagnostics can be obtained from the authors on request. The only model assumption not entirely satisfied was the normality of the residues, which were slight positively skewed. The model presented in Eq. (9) is not a QSPR model in the general sense, since it was not based on Fickian laws or assumptions, but was rather a statistical predictive model obtained from multiple linear regression using two readily accessible physicochemical properties and based on the notion that MW and log P may contain valuable information regarding the skin permeability potential of a chemical entity.

Since this model was built on variables bounded by specific ranges, we would need some way of determining whether a drug falls within these ranges. As a consequence of the mutual dependence between the variables used to construct Eq. (9), confidence intervals can be constructed for the estimated log *Kp*, MW and log P values.

2.6. Confidence interval determination

As mentioned in the previous subsection, the clade of groups 1 and 2 contains variables that are statistically dependent. MW, log P and log *Kp* are therefore covariates, and although this multicollinearity has a detrimental effect on how the model in Eq. (9) can explain its variance (as seen from the R^2 values), it does give us the ability to construct a confidence interval for the entire dataset, as well as marginalized confidence intervals for each pair of variables. Furthermore, the results from the cluster analysis estimated the densities of the variables to be normally distributed. The confidence interval for such an arrangement of variables does not take on the usual form, but rather that of an ellipsoid in three dimensions, the projection of which to plains of pairs of variables form 2D ellipses (Fig. 5), called a data/error ellipsoid and ellipses, respectively. The MW, log P data ellipse can therefore be used to determine whether or not a given drug falls within the range of statistically dependent MW and log P values.

Since the construction and testing of a data ellipsoid, or ellipse, requires some proficiency with matrix algebra, a computer program was written to do the necessary tests for the researcher. To maximize compatibility and user-friendliness, the program was written in the form of a visual basic for applications (VBA) subroutine, the source code of which is included in the supplementary information. This subroutine can be copied and pasted directly into an Excel VBA module without the need for any adjustments, and run from a spreadsheet using a command button. While a description of the mathematics behind the subroutine and general runtime conditions can be found in the experimental section, here we will only discuss the basic idea behind the tests performed by the subroutine.

The decision of whether or not a drug is within a specified MW, log P data ellipse is based on the "distance" of a drug's joint MW, log P value from the center of the ellipse. If this distance is less than or equal to the size, or "radius", of the ellipse, the drug will be within the region of statistical dependence. Important to note here is that the radius of a statistical ellipse is the same as a critical value, where *p* is the number of variables under investigation (see experimental section for an explanation). Therefore, to test how suitable a drug is for use in Eq. (9), its similarity to the data used to construct Eq. (9) is tested.

This test can be extended further, to include the estimated log *Kp* value. As stated above the MW, log P data ellipse is a marginalized MW, log P, log *Kp* data ellipsoid. The extra degree of freedom brought about by the inclusion of the log *Kp* variable can help decision making on borderline cases. From the application of these techniques to experimental data, in the next section, we shall show that failure of a drug to fall within the MW, log P data ellipses

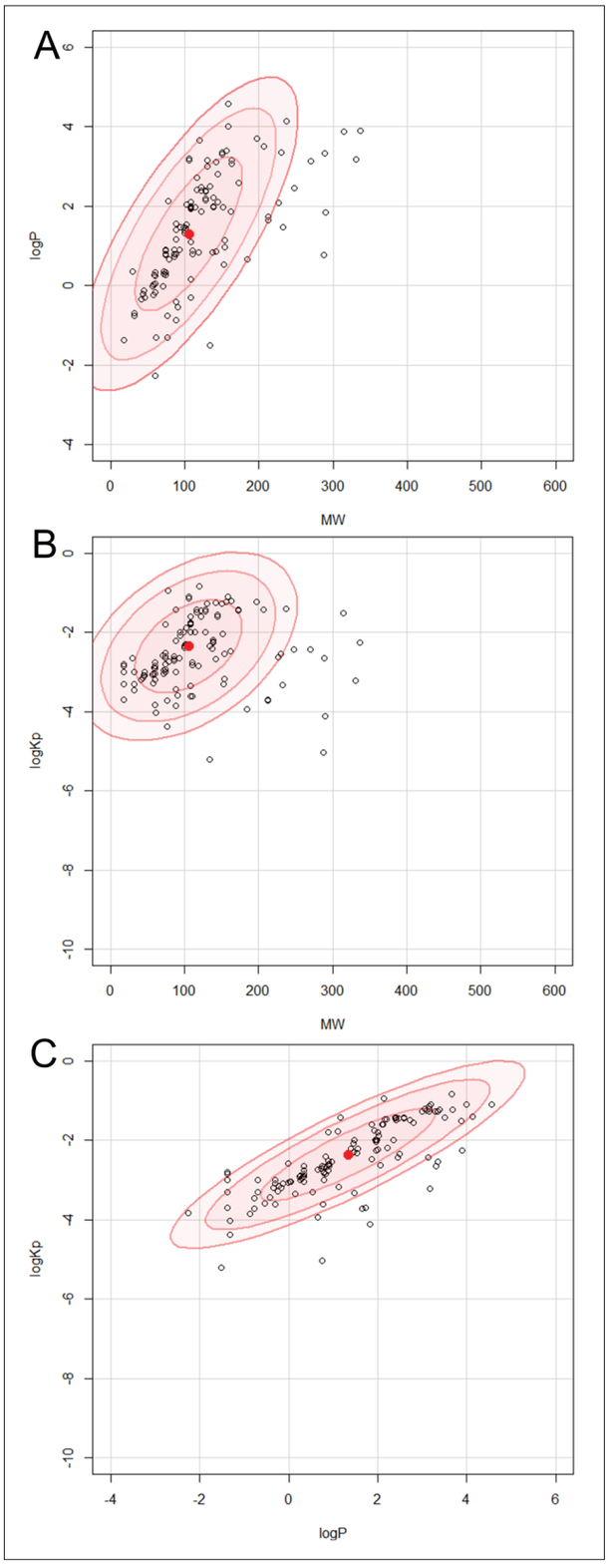

Fig. 5: Marginalized data ellipses of the combined groups 1 and 2, showing the 68 % (inner ellipse), 95 % and 99 % (outer ellipse) data ellipses.

does not necessarily mean that the estimated log *Kp* value will be inaccurate, only that less confidence can be placed in the estimate.

2.7. Application to experimental data

Figure 6 shows a screenshot of an Excel spreadsheet containing the names, MW and log P values of the NSAIDs tested in this study. It also gives a general layout of a spreadsheet that can incorporate the VBA subroutine using a command button. After execution of the subroutine, diclofenac sodium, mefenamic acid and piroxicam were determined to fall outside the 95 % data ellipse. However, upon inclusion of the estimated log *Kp* value, only diclofenac sodium and piroxicam remained outside the 95 % data ellipsoid. For both these drugs, MW made the largest contribution to their distances from the center and centroid of the data ellipse and ellipsoid, respectively. The small (in absolute value) log *Kp* value of mefenamic acid caused it to back fall inside the 95 % data ellipsoid, despite having fallen outside the 95 % data ellipse due to its large log P value. Both diclofenac sodium and mefenamic acid fall within the 99 % ellipsoid, while piroxicam still falls outside this interval. If the MW of diclofenac sodium is changed to that of its dissociated form (~295.15 Da), it also falls within the 99 % data ellipse. Therefore, with the exception of piroxicam, all the NSAIDs tested in this study are similar to at least 99 % of the dataset used to construct Eq. (9).

Table 3: Selected NSAIDs tested, their MWs, log P values, experimental and predicted skin permeability constants (in cm/s)

Drug	MW (g/mol)	Log P	Experimental log *Kp*		Predicted log *Kp*	
			PBS	Pheroid™	P&G	Eq.9
Ibuprofen	206.30	3.97	-1.262	-1.587	-4.739	-1.262
Ketoprofen	254.30	3.10	-1.424	-1.607	-5.650	-2.332
Diclofenac sodium	318.10	4.00	-2.373	-2.549	-5.400	-2.235
Mefenamic acid	241.30	5.12	-2.474	-3.162	-4.137	-0.724
Acetaminophen	151.20	0.64	-3.486	-3.318	-6.768	-3.233
Piroxicam	331.35	3.06	-3.931	-4.699	-6.149	-3.048

The NSAIDs, their physicochemical properties, experimentally determined and predicted log *Kp* values are also presented in Table 3. As a reference, the QSPR model of Potts and Guy (1992), abbreviated "P&G" in Table 3, was also used to predict log *Kp* values. The Potts and Guy equation was chosen because it contained the same variables as the model in Eq. (9) and had been shown to be the most accurate QSPR model (Lian et al. 2008).

Looking at the individual drugs, the predicted log *Kp* values of ibuprofen, ketoprofen, diclofenac sodium and acetaminophen, generated by Eq. (9), were much closer to the experimentally determined values. However, the prediction made by the Potts and Guy equation for mefenamic acid was better. This can be traced back to the structure of Eq. (9), where we can see that the log P intercept for drugs with MW = 241.3 is 6.1. Thus, for drugs with MW = 241.3, as log P approaches 6.1, log *Kp* approaches 0, which explains the small (in absolute value) log *Kp* value of mefenamic acid predicted by Eq. (9). Both Eq. (9) and the Potts and Guy equation gave poor predictions of piroxicam's log *Kp* value. For Eq. (9), this can be explained from the observation that piroxicam fell outside the 99 % data ellipse and ellipsoid (Fig. 6), largely due to its MW value, telling us that it is dissimilar to 99 % the data used to construct Eq. (9).

Overall, the predictions made by Eq. (9) appeared to be closer to the experimentally determined values. The mean squared error of the estimates for experimental and predicted, using Eq. (9), were 0.790 and 1.564, for the NSAIDs dissolved in PBS and dispersed in Pheroid™, respectively. For the experimental log *Kp* values and those predicted using the Potts and Guy equation, the mean squared error of the estimates were 9.595 and 8.227, for the NSAIDs dissolved in PBS and dispersed in Pheroid™, respectively. To supplement the forecasting error statistics, a Wilcoxon rank-sum test was performed as a nonparametric test of group differences. The results suggest that, at the 5% level of significance, the experimental log *Kp* values and those predicted from Eq. (9) were from identical populations with p-values = 0.4848 and 0.3095 for NSAIDs dissolved in PBS and dispersed in Pheroid™, respectively. It may also be concluded at the 5% level of significance that the experimental log *Kp* values and those predicted from the Potts and Guy equation were from nonidentical popula-

% data points to be included										
90	95	99		MW and log P			MW, log P and log Kp			Data ellipse tester
Drug name	MW	log P	log Kp	Radius	Distance	Test	Radius	Distance	Test	
Ibuprofen	206.3	3.97	-1.262	5.991	3.289	PASS	7.815	3.289	PASS	
Ketoprofen	254.3	3.1	-2.332	5.991	4.522	PASS	7.815	4.544	PASS	
Na diclofenac	318.1	4	-2.235	9.21	9.661	FAIL	11.345	9.690	PASS	
Mefenamic acid	241.3	5.12	-0.724	9.21	6.765	PASS	11.345	6.766	PASS	
Acetaminophen	151.2	0.64	-3.233	4.605	1.586	PASS	6.251	1.619	PASS	
Piroxicam	331.35	3.06	-3.048	9.21	12.951	FAIL	11.345	13.021	FAIL	

Fig. 6: Excel screenshot of the results from the "Data ellipse tester" VBA subroutine performed on the NSAIDs tested in this study. Ibuprofen and ketoprofen were tested against the 95 % interval, diclofenac sodium, mefenamic acid and piroxicam against the 99 % interval and acetaminophen against the 90 % interval.

tions, p-values = 0.0021 and 0.0043, respectively. Regardless of the differences in log *Kp* values between the NSAIDs dissolved in PBS and dispersed in Pheroid™, Eq. (9) was still able to give reasonable approximations of experimental log *Kp* values. Since the regression model in Eq. (9) is linear in its coefficients, it is still possible that negative log P values can cause a loss in predictive accuracy.

The results suggest that valuable information regarding the skin permeability of drugs can be found in MW and log P values, as long as the investigation is restricted to regions of statistical dependence.

3. Discussion

In this study, we investigated the probabilistic dependencies between log *Kp* and the two physicochemical properties most frequently used in skin permeability predictions, i.e. MW and log P. Initial observations based on a dataset constructed from several popular datasets used to construct and/or test predictive models, suggested that MW and log P are poorly correlated with log *Kp*. However, exploratory data analyses indicated the existence of regions of statistically significant dependence between these variables. As part of the analyses, a cluster analysis was performed on the dataset and two similar groups were identified, and used to construct a new, refined dataset. As an example of a possible application of the knowledge gained from the exploratory data analyses, a multiple linear regression model was constructed from this refined dataset and tested on experimental skin permeation data of selected NSAIDs. The regression model presented in this work (Eq. 9) gave reasonable approximations to experimental log *Kp* values. Since knowledge of whether a drug falls within the regions of statistical dependence is crucial to practical applications, e.g. Eq. (9), a method of testing the similarity between a given drug and those within the regions of dependence was presented.

Although MW and log P are not strongly correlated with log *Kp*, they remain the most frequently used predictors of skin permeability, are easily accessible and calculable, and have intuitive meaning in the transport process. By identifying and restricting investigations to regions of statistically significant dependence, valuable skin permeability information can be extracted from these physicochemical properties, and the confidence in predictions made regarding the skin permeability of compounds can be enhanced.

4. Experimental

4.1. Materials

The NSAIDs used in this study were donated by Adcock Ingram (South Africa). Analytical grade methanol, ethanol and phosphoric acid, PEG-400, as well as sodium chloride, disodium orthophosphate dehydrate, sodium dihydrogen orthophosphate dehydrate and dipotassium hydrogen orthophosphate anhydrous were purchased from Merck Laboratory Supplies (Midrand, South Africa). Double distilled deionized water was prepared with a Milli-Q water purification system (Millipore, Milford, USA). HPLC grade water was used throughout the study. Vitamin F ethyl ester was obtained from Chemimpo (Johannesburg, South Africa), Cremophor® RH40 from BASF (Midrand, South Africa) and dl-α tocopherol from DSM (Basel, Switzerland). The Pheroid™ used was prepared in-house by The Centre of Excellence for Pharmaceutical Sciences (Pharmacen) at the North-West University (Potchefstroom Campus, South Africa).

4.2. HPLC analysis

The high performance liquid chromatographic (HPLC) system used for the analysis was an Agilent 1100 series, equipped with a variable wavelength ultraviolet (UV) detector, isocratic pump, autosampler, and ChemStation (Rev. A.09.01 (1206)) data acquisition and analysis software. All analyses were performed using HPLC grade water and reactants. The temperature of the columns was kept at 25 °C throughout the analysis. All HPLC analyses were done, using a Phenomenex™ Luna 5 µ C_{18} (250 x 4.60 mm) column at a flow rate of 1 ml/min. All methods had previously been validated by the Analytical Technology Laboratory at the North-West University (Potchefstroom Campus). The NSAIDs (10 mg each) were accurately weighed and transferred into a 100 ml volumetric flask and made up to volume with PBS (pH of 7.4) to produce a 100.0 µg/ml stock solution. Dilutions with concentrations of 1.0; 2.5; 10.0; 25.0 and 100.0 µg/ml were prepared from the 100.0 µg/ml stock solution and used to construct a standard curve for solubility studies.

The solubility of each API included in this study, was determined in PBS (pH 7.4). All of the solubility determinations were done in triplicate. The Pheroid™ was prepared with PBS (pH 7.4) as dispersion medium. The samples were left to stir in a water bath at 32 °C for 24 h under supersaturated conditions. Each sample was then filtered through a 0.22 µm Millipore filter at 32 °C. The filtrate was then diluted and HPLC analysis was performed to determine the solubility.

Details on the chromatographic conditions and mobile phase compositions used in this study can be found in Table 4.

Table 4: Chromatographic conditions and mobile phase compositions used in this study

Drug	Mobile phase (acetonitrile/ water)	Retention time (min)	Wave length (nm)	Stop time (min)
Ibuprofen	65/35	6.0	225	8
Ketoprofen	65/35	2.5	260	5
Diclofenac sodium	65/35	3.9	277	5
Mefenamic acid	65/35	7.8	350	10
Acetaminophen	15/85	3.4	249	5
Piroxicam	65/35	2.9	340	5

4.3. Preparation of Pheroid™ vesicles

The Pheroid™ vesicles were prepared in-house at Pharmacen (North-West University, Potchefstroom Campus), by first mixing vitamin F ethyl ester (2.8% (w/v)), Cremophor® EL (1% (w/v)) and D-tocopherol (0.2% (w/v)). The mixture was heated to 75 °C to complete the oil phase of the vesicles. Purified water that had been saturated with N_2O was also heated and maintained at 75 °C. The vesicles were further prepared by adding the heated oil mixture to the N_2O saturated 75 °C water (96 %). The mixture was then homogenized, using a Heidolf Diax 600 homogenizer. The homogenous oil in water emulsion was then transferred and split into a number of amber glass bottles and each NDSAID added to a separate bottle. A previous study had shown that addition of a drug to the Pheroid™ during or after the manufacturing phase made little difference to the entrapment efficacy (Slabbert et al. 2011). These emulsions were continuously mechanically shaken, until room temperature was reached. The bottles, now containing Pheroid™ vesicles, were placed in a fridge and kept at 5 °C (Du Plessis et al. 2010).

4.4. Skin permeation experiments

Prior approval for the project, *in vitro* transdermal delivery of drugs through human skin, had been granted by the North-West University Ethics Committee (reference number NWU-00114-11-A5). Caucasian, female skin from informed consenting patients was obtained after cosmetic surgery. To minimize permeability variations among different skin, only abdominal skin was used. The full thickness skin was collected immediately after surgical removal and was prepared within 24 h post-surgery. The skin was rinsed with deionized water and blotted dry with clean tissue paper. To remove any residual fat from the subcutaneous fat layer and surface sebaceous lipids, the skin was carefully wiped once with an ethanol moistened cotton swab.

A skin layer 400 µm thick, including the stratum corneum, the viable epidermis and the upper dermis, with a width of 2.5 cm, was cut using a dermatome (Zimmer Inc., Warsaw, IN, USA). The prepared skin was placed dermal side down on filter paper. It was then wrapped in aluminum foil and frozen at -20 °C, until used. All skin samples were used within one month after preparation. An hour prior to commencing with the permeation experiments, the skin was removed from the freezer and thawed at room temperature and cut into circular pieces, 15 mm in diameter.

Vertically mounted Franz diffusion cells, each with a donor capacity of 1.0 ml and receptor capacity of 2.0 ml, were used. Preceding the permeation experiments, the integrity of the skin to be used was tested by measuring the electrical resistance across it, using a Tinsley LCR Databridge Model 6401 (Tinsley Precision Instruments, Croydon, United Kingdom) at 1 kHz, with a maximum voltage of 300 mV root-mean-square (rms) in the parallel equivalent circuit mode, by employing an alternating current (Fasano et al. 2002). After completion of the resistance measurements, the contents of the donor and receptor compartments were removed and cells with resistances of less than 10 kΩ were rejected. The effective diffusion area was calculated as 1.13 cm^2.

The PBS (pH 7.4) was degassed on an ultrasonic bath, prior to filling the receptor compartment. Care was taken to ensure that no air bubbles were trapped in the compartment or under the skin, as this would decrease the effective diffusion area. Each bottle of Pheroid™ with entrapped NSAID, was removed from the fridge and placed in a water bath at 32 °C under constant mechanical shaking prior to use.

The donor compartments were filled with 1 ml of Pheroid™ (experimental cells, n = 8), or 1 ml of the PBS (pH 7.4) solution (control cells, n = 7), each containing a different NSAID, and covered with Parafilm™ to prevent evaporation. The Pheroid™ delivery system was prepared by using the same dissolution medium as the control (PBS).

Sampling was done by removing the entire receptor phase at 20, 40, 60, 80 and 100 min, and at 2, 4, 6, 8, 10 and 12 h. After extraction, the receptor phase was immediately replaced with an equal volume of fresh PBS (pH 7.4), preheated to 37 °C, to maintain sink conditions. The concentration of the API that had penetrated the stratum corneum was recovered in the receptor compartment and after sampling analyzed by HPLC.

The skin permeation profiles of the different NSAIDs can be found in the supplementary information.

4.5. The dataset

The dataset used in this study was constructed by combining the datasets of Lian et al. (2008), Moss and Cronin (2002), and Wilschut et al. (1995), giving a total dataset size of n = 437. Many researchers have expressed concerns regarding the validity of the steroid data contained in the Flynn dataset (1990). For this reason the dataset of Moss and Cronin (2002), which incorporates updated steroid data, was chosen for this study.

4.6. A priori discretization of the dataset

Since a lower boundary for log P of 0 had been suggested (see introduction), and optimal values to be between 2 and 3, this was taken into account when deciding on the cut-off regions. Similarly, an upper MW boundary of 400 Da and optimal values at around 150 Da had been reported, and were incorporated in this study. Log *Kp* values above 1 correspond to exceptionally high *Kp* values, and are not expected to have a high frequency of occurrence, therefore this cut-off value was chosen as a region. Also, log *Kp* values below 7 correspond to extremely poor permeability and was used as a cut-off. For the middle regions of log *Kp*, the cut-off values were chosen in such a way as to not introduce a median split, and also to maintain the modes (see Fig. 1).

4.7. Statistical software

All data analyses were performed using R version 3.1.3 (2015-03-09), the R Foundation for Statistical Computing, Vienna, Austria, (http://www.R-project.org). Mosaic plots were constructed using the 'vcd' package in R and multivariate correspondence analysis was performed using the 'ca' package in R (Meyer et al. 2006; Zeileis et al. 2007; Nenadic and Greenacre 2007). Finally, cluster analysis was performed using the 'pdfCluster' package in R (Azzalini and Menardi 2014). The VBA subroutine was written in Microsoft Excel 2010.

4.8. Clustering analysis using nonparametric density estimation

Density estimation was done using the kernel method and calculated by a product estimator:

$$\hat{f}(y)=\sum_{i=1}^{n}\frac{1}{nh_{1,1}\cdots h_{i,d}}\prod_{j=1}^{d}K\left(\frac{y_j-x_{i,j}}{h_{i,j}}\right) \tag{10}$$

where K is the kernel function and hi is the bandwidth, which can either be fixed, $hi = h$, or adaptive, $hi = (hi,1 \cdots hi,d)^T$. The data was then clustered using the block-sequential criterion of allocation proposed by Azzalini and Torelli (2007), where for a fixed number of stages, K, an estimated density, $fm(xu)$, of the unallocated data xu was computed, based only on the data already allocated to group m, using the log-ratios:

$$r_m(x_u)=\log\frac{\hat{f}_m(x_u)}{\max_{l\neq m}\hat{f}_l(x_u)},\ \text{m=1,2,}\cdots\text{,M} \tag{11}$$

The density-based silhouette (*bds*) was used as a diagnostic tool to assess the quality of the clusters obtained from Eq. 10, and is defined as:

$$\text{dbs}_i=\frac{\log\left(\frac{\hat{\tau}_{m0}(x_i)}{\hat{\tau}_{m1}(x_i)}\right)}{\max_{x_i}\left|\log\left(\frac{\hat{\tau}_{m0}(x_i)}{\hat{\tau}_{m1}(x_i)}\right)\right|} \tag{12}$$

where *m0* is the group to which *xi* has been allocated and m_1 is the group for which $\tau m(xi)$ takes the second largest value. Therefore, large values of *dbs* are evidence of a well clustered data point, while small values indicate low confidence in the classification. The three clustering techniques employed were spatial tessellation with fixed and adaptive bandwidths and pairwise connections. The least amount of misclassified points was obtained from the adaptive bandwidth spatial tessellation technique, and therefore that technique was chosen for this study. A detailed list of which drugs in the dataset were classified into what groups can be found in the supplementary information. The *dbs* values were appreciably higher than zero, suggesting that the partitions identified were sound (see supporting information).

4.9. Data ellipse and ellipsoid determination

The VBA subroutine, which can be found in the supplementary information, was built around the following mathematical principles.

If we let be the mean vector of the properties investigated in this study, i.e. where is the mean value of MW, the mean value of log P and the mean value of log *Kp*, then we can recognize the squared Mahalanobis distance between a point and the centroid of the sample as being,

$$D_M^2(\boldsymbol{y})=(\boldsymbol{y}-\overline{\boldsymbol{y}})^T S^{-1}(\boldsymbol{y}-\overline{\boldsymbol{y}}) \tag{13}$$

Where S^{-1} is the sample covariance matrix, and can be computed as

$$S=(n-1)^{-1}\sum_{i=1}^{n}(\boldsymbol{y}_i-\overline{\boldsymbol{y}})(\boldsymbol{y}_i-\overline{\boldsymbol{y}}^T) \tag{14}$$

The squared Mahalanobis distance can be substituted into the matrix form of the ellipsoid equation to define a data ellipsoid, of size, or "radius", *r*, which represents the set of all points than have a squared Mahalanobis distance less than or equal to *r2*, and can be written as

$$\mathcal{E}_c(\overline{\boldsymbol{y}},S):=\left\{y:(\boldsymbol{y}-\overline{\boldsymbol{y}})^T S^{-1}(\boldsymbol{y}-\overline{\boldsymbol{y}})\leq r^2\right\} \tag{15}$$

An important result here is that, since the variables are multivariate normal distributed, will be distributed, where *p* is it number of variables (Friendly et al. 2013).

The mean values and covariance matrices of the variables in groups 1 and 2 were pre-programmed into the subroutine. Therefore, only the MW and log P values of the drug(s) under investigation are needed to perform the test. Following a similar spreadsheet layout as in Fig. 6, the subroutine will first ask for the drug's name, properties and the % of data points within which the drug is expected to fall. It then estimates the log *Kp* value using Eq. (9), and returns the "radii" of the data ellipse and ellipsoid, as well as the distance of the drug from the center and centroid of the data ellipse and ellipsoid, respectively. Finally it returns the result of the test, indicating whether or not the drug under investigation is within the specified data ellipse and ellipsoid.

Acknowledgements: This work was carried out with the financial support of the National Research Foundation of South Africa (NRF) (Grants no. IFRR81178 and CPRR13091742482) and The Centre of Excellence for Pharmaceutical Sciences (Pharmacen) of the North-West University, Potchefstroom Campus, South Africa.

Disclaimer: Any opinion, findings and conclusions, or recommendations expressed in this material are those of the authors and therefore the NRF does not accept any liability in regard thereto.

References

Abraham MH, Chadha HS, Mitchell RC (1995) The factors that influence skin penetration of solutes. J Pharm Pharmacol 47: 8 – 16.

Amidon GL, Lennernas VP, Shah JR, Crison A (1995) A theoretical basis for a biopharmaceutic drug classification: the correlation of in vitro drug product dissolution and in vivo bioavailability. Pharm Res 12: 413 – 420.

Azzalini A, Menardi G (2014) Clustering via Nonparametric Density Estimation: The R Package pdfCluster. J Stat Softw 57: 1 – 26.

Azzalini A, Torelli N (2007) Clustering via nonparametric density estimation. Stat Comput 17: 71 – 80.

Barratt MD (1995) Quantitative structure-activity relationships for skin permeability. Toxicol In Vitro 9: 27 – 37.

Barry BW (2001) Novel mechanisms and devices to enable successful transdermal drug delivery. Eur J Pharm Sci 14: 101 – 114.

Bharate SS, Vishwakarma RA (2013) Impact of preformulation on drug development. Expert Opin Drug Deliv 10: 1239 – 1257.

Bos JD, Meinhardi MMHM (2000) The 500 Dalton rule for skin penetration of chemical compounds and drugs. Exp Dermatol 9: 165 – 169.

Bouwman T, Cronin MTD, Bessems JGM, van de Sandt JJM (2008) Improving the applicability of (Q)SARs for percutaneous penetration in regulatory risk assessment. Hum Exp Toxicol 27: 269-276.

Chen Y, Yang WL, Matheson LE (1993) Prediction of flux through polydimethylsiloxane membranes using atomic charge calculations. Int J Pharm 94: 81 – 88.

Choy YB (2011) The rule of five for non-oral routes of drug delivery: Ophthalmic, inhalation and transdermal. Pharm Res 28: 943 – 948.

Cooper ER (1986) Molecular modifications for dermal and transdermal drug delivery. Pharm Int 7: 308 – 310.
Du Plessis LH, Lubbe J, Strauss T, Kotzé AF (2010) Enhancement of nasal and intestinal calcitonin delivery by the novel Pheroid™ fatty acid based delivery system and by N-trimethyl chitosan chloride. Int J Pharm 385: 181 – 186.
Fasano WJ, Manning LA, Green JW (2002) Rapid integrity assessment of rat and human epidermal membranes for *in vitro* regulatory testing: correlation of electrical resistance with tritiated water permeability. Toxicol In Vitro 16: 731 – 740.
Fitzpatrick D, Corish J, Hayes B (2004) Modelling skin permeability in risk assessment – the future. Chemosphere 55: 1309 – 1314.
Flynn GL (1990) Physicochemical determinants of skin absorption. In: Gerity TR, Henry CJ (eds.) Principles of route-to-route extrapolation for risk assessment. Amsterdam, Elsevier, p. 93 – 127.
Frasch HF (2002) A random walk model of skin permeation. Risk Anal 22: 265 – 276.
Friendly M, Monette G, Fox J (2013) Elliptical insights: Understanding statistical methods through elliptical geometry. Stat Sci 28: 1-39.
Hadgraft J, Lane ME (2005) Skin permeation: The years of enlightenment. Int J Pharm 305: 2 – 12.
Hartemink A. Principled computational methods for the evaluation and discovery of genetic regulatory networks [Ph.D. thesis], Massachusetts Institute of Technology, Cambridge, MA, 2001.
Le VH, Lippold BC (1995) Influence of physicochemical properties of homologous esters of nicotinic acid on skin permeability and maximum flux. Int J Pharm 124: 285 – 292.
Lian G, Chen L, Han L (2008) An evaluation of mathematical models for predicting skin permeability. J Pharm Sci 97: 584 – 598.
Lien EJ, Gao H (1995) Qsar analysis of skin permeability of drugs in man as compared to *in vivo* and *in vitro* studies in rodents. Pharm Res 12: 583 – 587.
Lipinski CA, Lombardo F, Dominy BW, Feeney PJ (2001) Experimental and computational approaches to estimate solubility and permeability in drug discovery and development settings. Adv Drug Deliv Rev 46: 3 – 26.
Lippold BC (1991) How to optimize drug penetration through skin. Pharm Acta Helv 67: 294 – 300.
Magnusson BM, Anissimov YG, Cross SE, Roberts MS (2004) Molecular size as the main determinant of solute maximum flux across the skin. J Invest Dermatol 122: 993 – 999.
Magnusson BM, Pugh WJ, Roberts MS (2004) Simple rules defining the potential of compounds for transdermal delivery or toxicity. Pharm Res 21: 1047 – 1054.
Menardi G, Azzalini A (2014) An advancement in clustering via nonparametric density estimation. Stat Comput 24: 753 – 767.
Meyer D, Zeileis A, Hornik K (2006) The strucplot framework: visualizing multi-way contingency tables with vcd. J Stat Softw 17: 1 – 48.
Mitragotri S (2002) A theoretical analysis of permeation of small hydrophobic solutes across the stratum corneum based on scaled particle theory. J Pharm Sci 91: 744 – 752.
Mitragotri S (2003) Modeling skin permeability to hydrophilic and hydrophobic solutes based on four permeation pathways. J Control Rel 86: 69 – 92.
Moss GP, Cronin MTD (2002) Quantitative structure-permeability relationships for percutaneous absorption: re-analysis of steroid data. Int J Pharm 238: 105 – 109.
Moss GP, Dearden JC, Patel H, Cronin MTD (2002) Quantitative structure-permeability relationships (QSPRs) for percutaneous absorption. Toxicol In Vitro 16: 299-317.
Nenadic O, Greenacre M (2007) Correspondence analysis in R, with two- and three-dimensional graphics: The ca package. J Stat Softw 20: 1 – 13.
Potts RO, Guy RH (1992) Predicting skin permeability. Pharm Res 9: 663 – 669.
Potts RO, Guy RH (1995) A predictive algorithm for skin permeability - the effects of molecular-size and hydrogen-bond activity. Pharm Res 12: 1628 – 1633.
Roy SD (1997) Preformulation aspects of transdermal drug delivery systems. In: Ghosh TK, Pfister WR, Yum SI (eds.) Transdermal and topical drug delivery systems. Buffalo Grove, Illinois, Interpharm Press. p. 139 – 166.
Saunders, JCJ, Davis, HJ, Coetzee, L, Botha, S, Kruger, AE, Grobler, A (1999) A novel skin penetration enhancer: elevation by membrane diffusion and confocal microscopy. J Pharm Pharm Sci 2: 99 – 107.
Scheuplein RJ (1965) Mechanism of percutaneous absorption. I. Routes of penetration and the influence of solubility. J Invest Dermatol 45: 334 – 346.
Shen J, Kromidas L, Shultz T, Bhatia S (2014) An *in silico* skin absorption model for fragrance materials. Food Chem Toxicol 74: 164 – 176.
Slabbert C, Du Plessis LH, Kotzé AF (2011) Evaluation of the physical properties and stability of two lipid drug delivery systems containing mefloquine. Int J Pharm 409: 209 – 215.
Wiedersberg S, Guy RH (2014) Transdermal drug delivery: 30 + years of war and still fighting! J Control Release 190: 150 – 156.
Wilscut A, Ten Berge WF, Robinson PJ, McKone, TE (1995) Estimating skin permeation. The validation of five mathematical skin permeation models. Chemosphere 30: 1275 – 1296.
Zeileis A, Meyer D, Hornik K (2007) Residual-based shadings for visualizing (conditional) independence. J Comp Graph Stat 16: 507 – 525.